Sensors & Actuators: B. Chemical 318 (2020) 128223

Contents lists available at ScienceDirect

Sensors and Actuators B: Chemical

journal homepage: www.elsevier.com/locate/snb

Scalable metal oxide functionalized GaN nanowire for precise SO_2 detection

Md Ashfaque Hossain Khan[a,*], Brian Thomson[b], Jie Yu[b], Ratan Debnath[b], Abhishek Motayed[b], Mulpuri V. Rao[a,*]

[a] Department of Electrical and Computer Engineering, George Mason University, Fairfax, VA 22030, USA
[b] N5 Sensors, Inc., Rockville, MD 20850, USA

ARTICLE INFO

Keywords:
Gas sensor
GaN nanowire
Metal-oxide
Sulfur dioxide (SO_2)
Sensitivity
Selectivity

ABSTRACT

In this work, GaN nanowires have been formed on Si substrate using production standard stepper lithography and top-down approach. Three different functionalized devices were prepared by the deposition of metal oxides-ZnO, WO_3 and SnO_2 by optimized RF sputtering on nanowires followed by rapid thermal annealing. The elemental composition, crystallinity and surface topography of metal-oxide/GaN nanowires were fully characterized by EDS, XRD, AFM and SEM. The SO_2 gas sensing data was collected and analyzed for all three sensors. The ZnO/GaN sensor was found to be the best candidate for precise SO_2 detection. To examine the real-world applicability of ZnO/GaN sensor device, its additional sensing properties, including gas sensing adsorption and desorption rate, cross-sensitivity to interfering gases, and long-term stability at various environmental conditions were investigated. Furthermore, principal component analysis has been performed to address the cross-sensitive behavior of ZnO. The SO_2 sensing mechanism on metal-oxide/GaN under UV irradiation was discussed as well. Results demonstrate that ZnO functionalized GaN nanowire can be employed as a high performance SO_2 sensor.

1. Introduction

The US Environmental Protection Agency (US EPA) and others have long recognized the environmental and public health significance of air pollutants like SO_2, one of the six pollutants regulated under the US National Ambient Air Quality Standards (NAAQS). The one-hour exposure limit has been set 75 ppb for SO_2 by the standards [1]. The prime sources of SO_2 include burning of fossil fuels in oil refineries, power stations, industrial plants and motor vehicles [2]. It is also produced during the processing of mineral ores containing sulfur, as well as from natural sources like active volcanoes and forest fires. Excessive SO_2 exposure is detrimental to the health of eyes, lungs and throat [3]. SO_2 gas molecules easily dissolve in the water droplets in clouds, causing acid rain that affects natural balance of rivers, lakes and soils, resulting in damage to wildlife and vegetation [4]. Combining with air moisture, it causes gradual damage to some building materials (e.g., limestone) as well.

In comparison to gas detection techniques like optical [5], acoustic [6], and gas chromatographic methods [7] functionalized nano-structured semiconductors have been highly effective due to the advantages such as- low energy linear output with high resolution, lower aspect-ratio, repeatability, ppm level detection with high accuracy, and lower cost [8,9]. However, semiconductor-based sensors are highly sensitive to temperature and humidity fluctuations and have minimal shell life [10]. Therefore, further research efforts are required to explore novel semiconducting materials and develop robust gas sensors for reliable SO_2 detection.

Over the past few years, several highly-sensitive SO_2 gas sensors were reported using various nanostructured semiconducting materials including graphene [11], MoS_2 [12], SnO_2 [13], NiO-ZnO [14], and $SrMoO_4$ [15]. However, when it comes to robust and reliable SO_2 detection, nanostructured GaN is an attractive semiconducting backbone material. Having a direct large band gap of 3.4 eV, GaN exhibits the ability to operate at a wide range of temperatures, provide radiation and environmental stability, and mechanical robustness [16].

One-dimensional (1D) nanowire-based sensors have been extensively used to detect several gas species at extremely low concentrations due to their large surface-to-volume ratio [17]. Though nanowires are electrically sensitive, they exhibit poor selectivity due to inadequate and non-specific adsorption [18,19]. It is well known that nanowire selectivity toward analyte can be improved by catalytic functionalization. Very few experimental chemical sensing results of functionalized GaN nanowires have been reported previously [20,21].

In this paper, we have presented three different SO_2 gas sensors based on ZnO, WO_3 and SnO_2 functionalization of GaN nanowires formed using top-down fabrication approach. From now on, for

* Corresponding authors.
E-mail addresses: mkhan53@gmu.edu (M.A.H. Khan), rmulpuri@gmu.edu (M.V. Rao).

https://doi.org/10.1016/j.snb.2020.128223
Received 21 November 2019; Received in revised form 27 April 2020; Accepted 28 April 2020
Available online 13 May 2020

convenience, in the main body of the paper we refer the devices only using the type of metal oxide, because GaN nanowire is the common backbone for all sensor devices of this study. As-prepared sample morphologies, microstructures, and compositions were fully characterized via X-ray diffraction (XRD), energy dispersive spectroscopy (EDS), scanning electron microscopy (SEM) and atomic force microscopy (AFM). The room-temperature SO_2 sensing properties of the devices were investigated, and ZnO functionalized GaN nanowire was found to be the optimal SO_2 sensor among the considered metal oxide coated sensors. For further confirmation of ZnO/GaN nanowire as an appropriate SO_2 detector, its additional sensing properties, including selectivity, repeatability, and long-term stability were evaluated. Furthermore, the basic SO_2 sensing mechanism of metal oxide functionalized GaN nanowire has been discussed.

2. Experimental details

2.1. Sensor materials

The GaN on silicon wafers were purchased from EpiGaN. All the metal-oxide sputtering targets were obtained from Kurt J. Lesker company.

2.2. Sensor fabrication

The proposed sensor devices have been fabricated using the standard fabrication technique in a class 100 cleanroom. The schematic process flow for the sensor fabrication is illustrated in Fig. 1. After doing standard RCA cleaning, GaN nanowires of width 300–400 nm have been formed by stepper lithography assisted dry etching. While performing inductively coupled plasma (ICP) etching, patterned metal was used to protect the defined GaN nanowire. Then, ohmic contacts were formed on nanowire ends with a deposition sequence of Ti (40 nm)/Al (80 nm)/Ti (40 nm)/Au (40 nm) in a standard electron beam evaporator. After that, SiO_2 layer was deposited on the device by plasma-enhanced chemical vapor deposition (PECVD) to protect the nanowire and metal contacts from being damaged during high temperature processing and etching. Next, reactive ion etching (RIE) was employed to create an active area on nanowire for the functionalization by metal oxide. Three different metal oxides, such as- ZnO, WO_3 and SnO_2 were deposited on the exposed GaN nanowires using RF magnetron sputtering. These physical vapor depositions were performed in a reactive atmosphere with O_2 flow at 300 °C and 280 W RF power. Then, rapid thermal annealing (RTA) was performed in pure Ar at 600 − 700 °C for 4–5 min in order to crystallize the deposited metal oxides and to enhance the ohmic contacts to the GaN nanowires. Later, metal bond pads with a sequence of Ti (40 nm) and Au (150 nm) were deposited upon ohmic metal contacts in the electron beam evaporator. After completing the above-described steps, sensor devices were mounted on and wire bonded to a 24-pin ceramic dual in line (DIP) package.

2.3. Instruments and experimental set-up

The microstructures and surface morphologies of the fabricated metal-oxide/GaN sensors were characterized by field-emission scanning electron microscopy (FESEM). The synthesized samples were examined in a Zeiss Ultra 60 Field Emission Scanning Electron Microscope. The elemental components of the synthesized GaN nanowire were verified through energy-dispersive X-ray spectroscopy (EDS). The crystallinity and phase of the metal oxide films were examined by X-ray diffraction (XRD) using a Rigaku Smart Lab X-ray diffraction system having Cu-Kα radiation. The advanced surface topography and roughness of the prepared metal-oxide/GaN sensors were studied by an Asylum Cypher High Resolution Atomic Force Microscope.

The UV illuminated current-voltage measurements of the fabricated

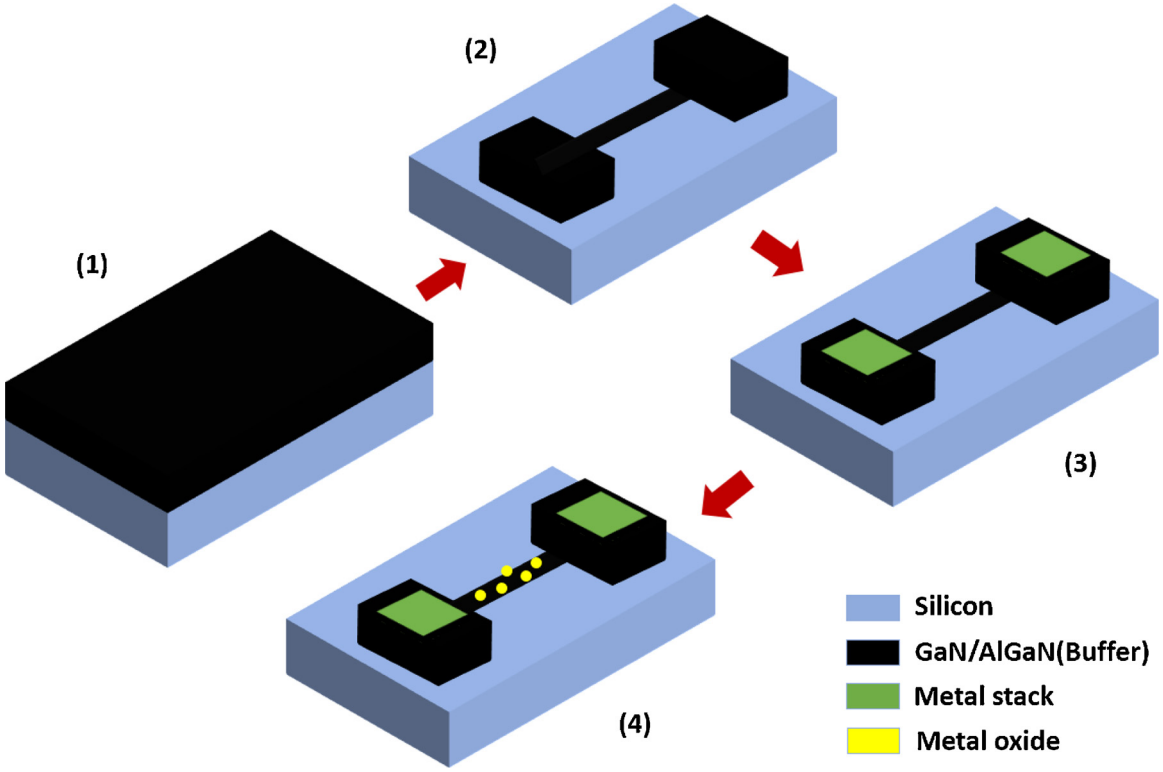

Fig. 1. Schematic process flow for the proposed sensor fabrication. (1) Standard RCA cleaning of GaN wafer before lithographic pattern transfer. (2) Implementation of stepper lithography and ICP etching to develop GaN nanowires on Si substrate. (3) Ohmic contact formation between metal stack and GaN. (4) Deposition of metal oxide on nanowire for surface functionalization.

devices were performed by a National Instrument PCI DAQ system. Light emitting diode (LED) UV light source was used having a wavelength of 365 nm with output power was maintained at 470 mW/cm^2. The devices were placed in a custom designed gas chamber made of stainless steel for gas sensing data collection. A mixture of SO_2 gas and compressed breathing air was flowed into the sensing chamber and the net flow (air + SO_2) was maintained at 0.5 slpm. Mass flow controllers (MFCs) independently controlled the flow rate of each component, determining the composition of the mixed gas. The sensor currents were measured by the National Instrument PCI DAQ system by applying a constant 5 V DC voltage. The device had been allowed to regain the baseline current without purging the gas chamber after SO_2 exposure. Sensor response is calculated as $(R_{gas} - R_{air})/R_{air}$, where R_{gas} and R_{air} are the resistances of the sensor in the presence of the analyte–air mixture and in the presence of air, respectively. Finally, long-term stability study was conducted on the fabricated devices under various environmental conditions in a Tenny BTRC temperature and humidity test chamber.

3. Results and discussion

3.1. Material and device characterizations

A buffer layer of $Al_{0.25}Ga_{0.75}N$ was formed in between GaN layer and Si substrate to minimize the lattice mismatch. Fig. 2(a) shows EDS spectra of the fabricated GaN/AlGaN nanowire on Si substrate. The existence of elemental components, such as- Ga, Al and N on the substrate are clearly verified by the corresponding EDS peaks.

Since metal-oxide functionalized GaN NWs are minute in size, reference samples with ZnO, WO_3 and SnO_2 thin films on sapphire substrate were prepared to detect the XRD signals. The considered metal oxides were deposited on the substrate by RF magnetron sputtering to form a 40 nm thin film. The deposition was followed by annealing at 600 − 700 °C for 4 − 5 min with the supposition that an identical metal oxide morphology has been formed on the substrate as in the metal oxide coated GaN NW case. Fig. 2(b) presents the XRD spectrum of the prepared ZnO thin film where diffraction peaks are indexed to ZnO with a hexagonal wurtzite crystal structure (JCPDS: 36-1451). A strong growth orientation along (002) plane suggests that the film growth is perpendicular to the substrate [22]. Due to possessing least surface energy, the (002) plane of ZnO is thermodynamically favorable [23]. The weak diffraction peaks corresponding to the (101), (102), and (103) planes reveals the existence of few randomly oriented grains. The XRD pattern of annealed WO_3 thin film is shown in Fig. 2(c). The major diffraction peaks are exhibited at 23.84, 33.74, 41.76, and 48.65°, which are attributed to the planes (002), (202), (122) and (222) of hexagonal WO_3 (JCPDS: 32-1395). Fig. 2(d) shows the XRD patterns obtained from SnO_2 thin film sample after annealing in a similar process. As seen from the detected diffraction pattern of SnO_2, the peaks corresponding to (110), (101), (200), (211), (220), and (002) planes

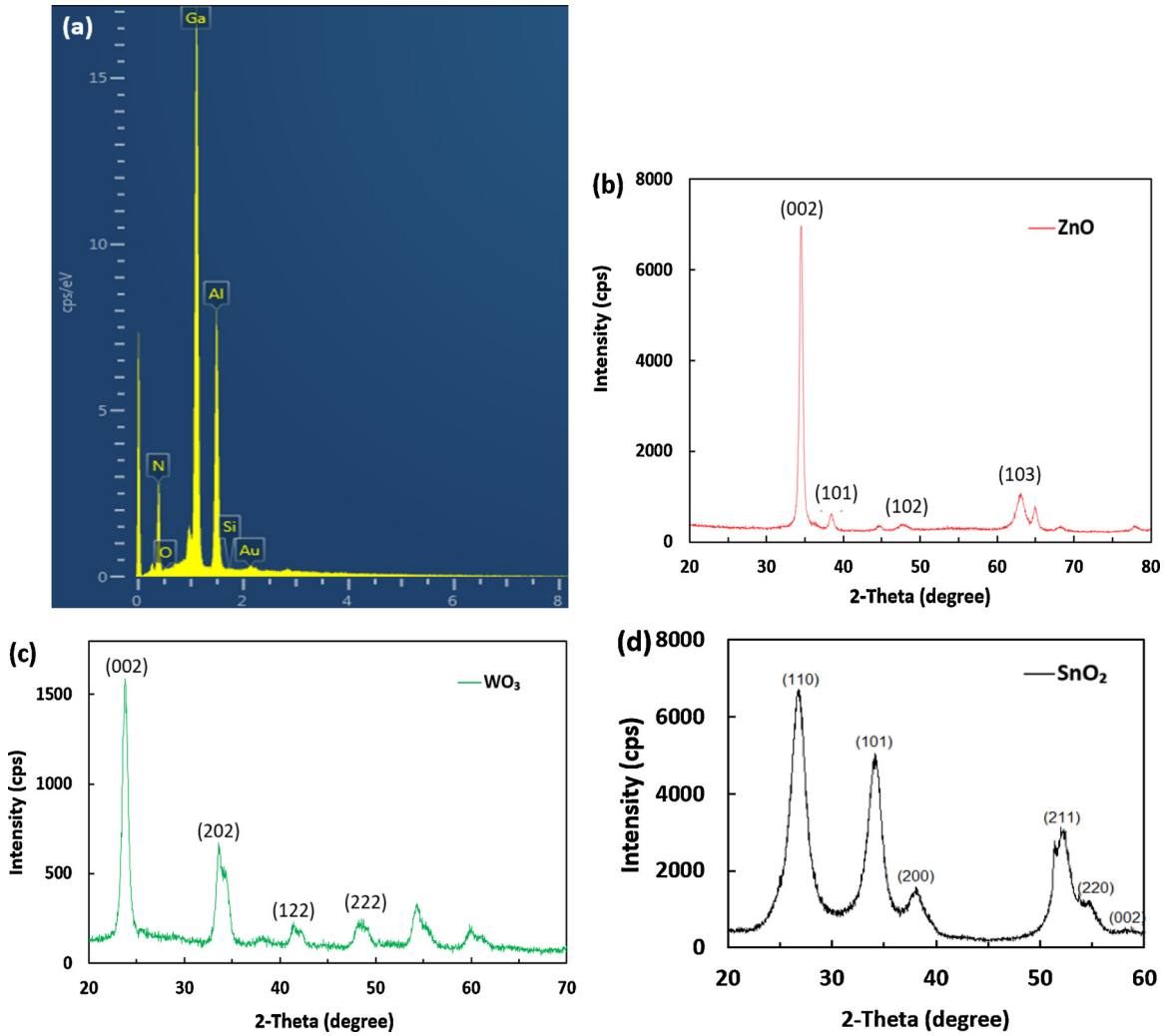

Fig. 2. (a) EDS spectra of the fabricated GaN/AlGaN nanowire on Si substrate. X-ray diffraction patterns of (b) ZnO thin film, (c) WO_3 thin film, and (d) SnO_2 thin film on sapphire substrate.

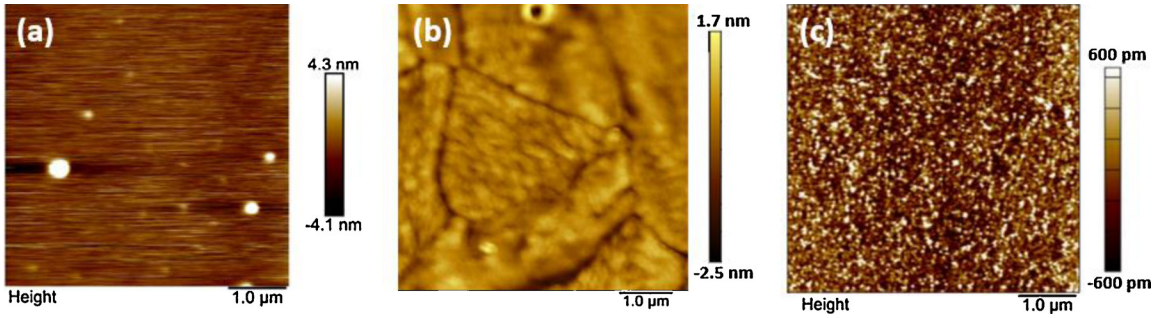

Fig. 3. High-resolution 2D AFM images of the annealed (a) ZnO, (b) WO_3, and (c) SnO_2 on sapphire substrate.

indicate the presence of cassiterite crystal phase with tetragonal structure (JCPDS: 41-1445). Lack of sharpness of the peaks reveals the polycrystalline nature of the SnO_2 film.

Minor dislocations in few XRD peak positions are caused by the residual stress within the film due to a mismatch in thermal expansion coefficients of the metal oxides and sapphire substrate. The average crystallite size (D) was estimated using the following Debye-Scherrer equation [24]:

$$D = \frac{0.9\lambda}{\beta \cos\theta} \quad (1)$$

where D is the crystallite size, λ is the X-ray wavelength, β is the full width at half maximum of the diffraction peak, and θ is the Bragg diffraction angle of the peaks. The average crystallite sizes were found to be 18.51 nm, 30.80 nm and 17.45 nm for the ZnO, WO_3 and SnO_2 thin films, respectively.

The topography and roughness of the fabricated metal oxides coated GaN nanowires are illustrated using two-dimensional Atomic force microscopy (AFM) images as shown in Fig. 3(a–c). The root mean square (rms) surface roughness of ZnO, WO_3 and SnO_2 thin films are found to be 4.21 nm, 3.95 nm and 1.4 nm, respectively. The moderate surface roughness of these deposited metal oxides contributes to a larger sensing response than those of highly uniform surfaces towards the analyte gas molecules. However, excessive surface roughness hampers response and recovery rates due to decreased self-diffusivity of analyte molecules [25].

Fig. 4(a) shows FESEM image of the fabricated GaN nanowire after forming ohmic metal contacts on the two ends. The morphologies of the nanowire were observed quite uniform exhibiting a height and width of 300 ± 20 nm and 400 ± 8 nm, respectively. The UV illuminated current–voltage (I–V) characteristics of the fabricated devices are presented in Fig. 4(b). It is seen that bare GaN nanowire exhibits lower conductivity before functionalizing with metal oxide. This phenomenon is attributed to the introduction of surface states on GaN through ambient oxygen adsorption [26]. All three metal-oxide functionalized GaN devices showed linear I –V characteristics, indicating the formation of ohmic contacts to sensor devices.

3.2. Gas sensing properties

The dynamic response-recovery curves for the three considered metal-oxide/GaN nanowire-based sensor devices on exposure to 0.5, 1, 10, 100 and 500 ppm concentrations of SO_2 gas are shown in Fig. 5. In the case of bare GaN nanowire, SO_2 response is very weak compared to the metal-oxide functionalized GaN sensors even at high concentrations (not shown). All the gas sensing data was collected in dry air under UV light at room temperature (20 °C). Under the irradiation of UV light, the metal-oxide nanocluster photo-desorbs water and oxygen creating surface defect active sites and electron-hole pairs are generated in the GaN backbone [27]. The target SO_2 molecules are chemisorbed at those generated active sites. Then dynamic trapping and de-trapping of charge carriers at those active sites by the adsorbed molecules causes surface potential modification of the GaN backbone, leading to modulation of the sensor current, which is proportional to the SO_2 concentration.

The higher magnitude response-curve with steeper slope under UV irradiation indicates the contribution of UV light to the enhancement of the gas sensing response (Supplementary Material). Each sensor had been allowed to obtain a stable baseline signal by flowing only dry air for 10 min. before exposing to the analyte gas for 250 s. When SO_2 gas flow was turned off, the sensor was kept for 10 min. for baseline recovery without any purging. It was clearly seen that ZnO sensor responded the highest in magnitude among the three sensors for all test concentrations. The sensors with other two functionalizing metal oxides exhibited significant gas responses as well.

The normalized responses of the three metal-oxide/GaN sensors are plotted as a function of SO_2 gas concentration in Fig. 6. The fitting equations of the sensor response Y and gas concentration X are stated as $Y = 1.954 \ln X + 6.260$, $Y = 1.001 \ln X + 3.382$ and $Y = 0.483 \ln X + 0.993$ for ZnO, WO_3 and SnO_2 sensor devices, respectively, and the

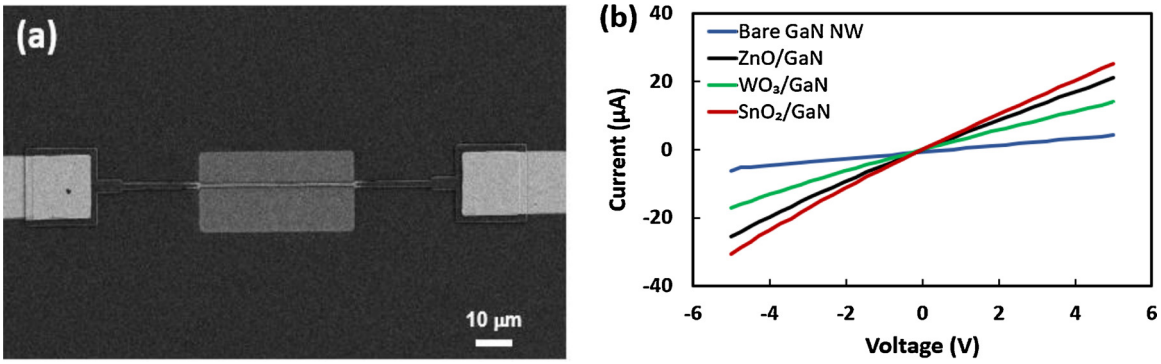

Fig. 4. (a) FESEM image of the developed bare GaN nanowire. (b) I–V characteristics of the GaN nanowire devices functionalized with different metal oxides in presence of UV light.

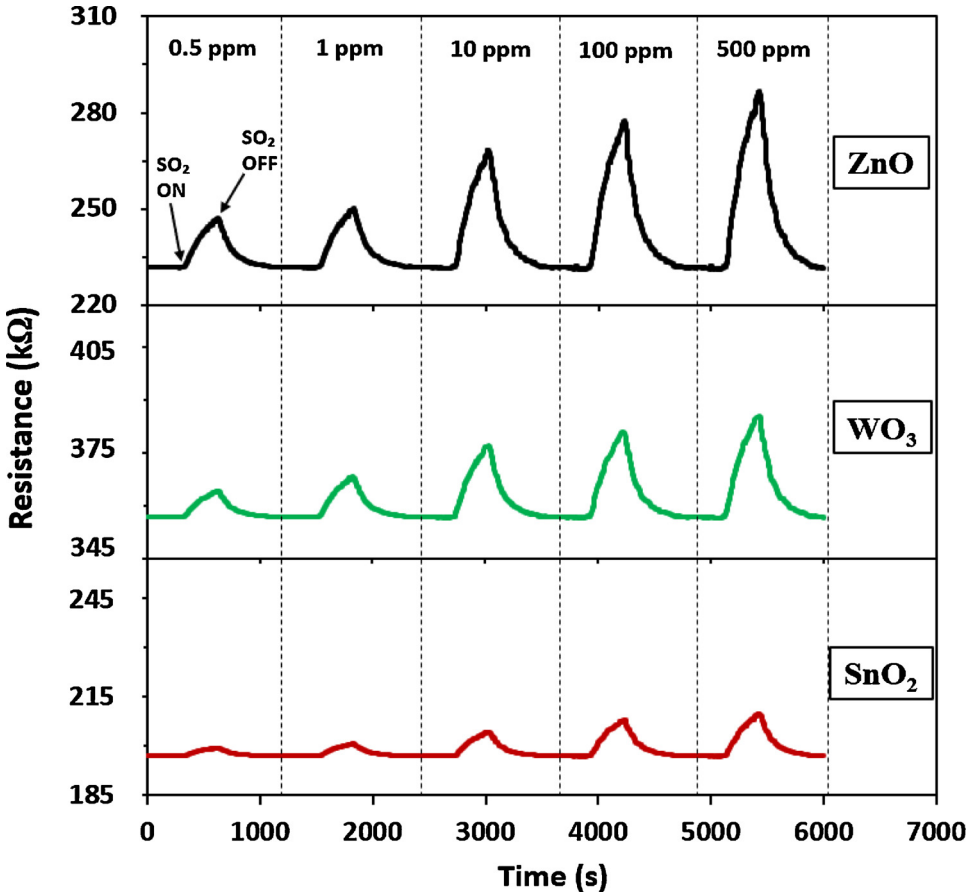

Fig. 5. Resistance responses of the ZnO/GaN device, WO_3/GaN device and SnO_2/GaN device for varying concentrations of SO_2 gas in dry air under UV light at room temperature (20 °C).

regression coefficient is 0.9812, 0.9562, and 0.9165, respectively. The largest coefficients within the fitting equation and highest regression coefficient of ZnO device confirms that it possesses the highest sensitivity and excellent sensing linearity to our target analyte. Yamazoe et. al. showed that the electric resistance of a semiconductor gas sensor under exposure to a target gas is proportional to P^n, where P is partial pressure of the gas and n is a constant specific to the kind of target gas [28]. Here, in case of oxidizing SO_2 gas, the power law exponent has been derived as 3.1 from response vs gas concentration data for the ZnO/GaN device by utilizing all the standard values of the parameters specified in that paper.

The response time is defined as the time taken by a sensor response to reach 90 % of the total response change when exposed to the analyte. Similarly, recovery time is the time taken by a sensor response to reach 90 % of the total response change when analyte is turned off. Fig. 7(a–c) depicts SO_2 gas response/recovery process of ZnO, WO_3 and SnO_2 sensors when exposed to 10 ppm SO_2 in dry air under UV light at room temperature (20 °C). It was found that ZnO device was the fastest in SO_2 response among the three considered sensors due to substantial chemical interaction between ZnO and SO_2 molecules as revealed from the

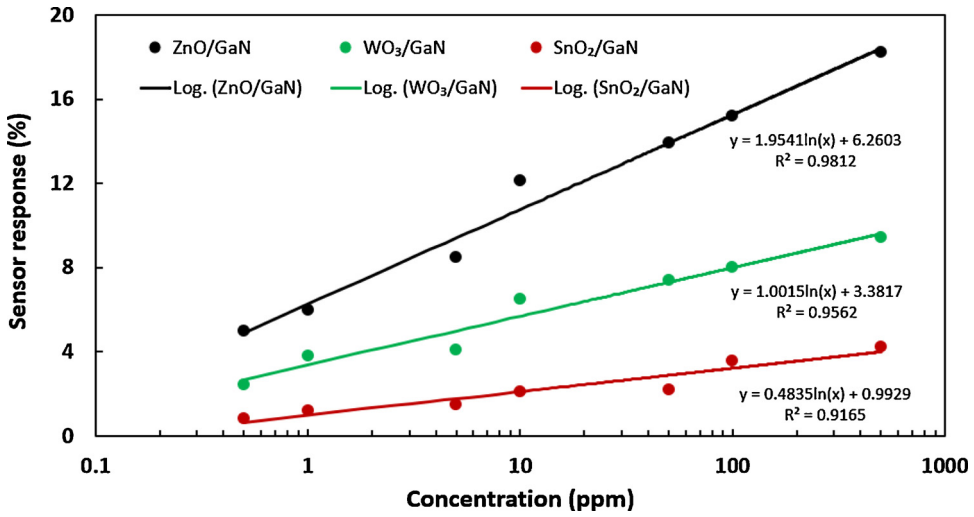

Fig. 6. Response fitting lines of the ZnO/GaN device (black), WO_3/GaN device (green) and SnO_2/GaN device (red) for varying concentrations of SO_2 gas in dry air under UV light at room temperature (20 °C). (For interpretation of the references to colour in this figure legend, the reader is referred to the web version of this article.)

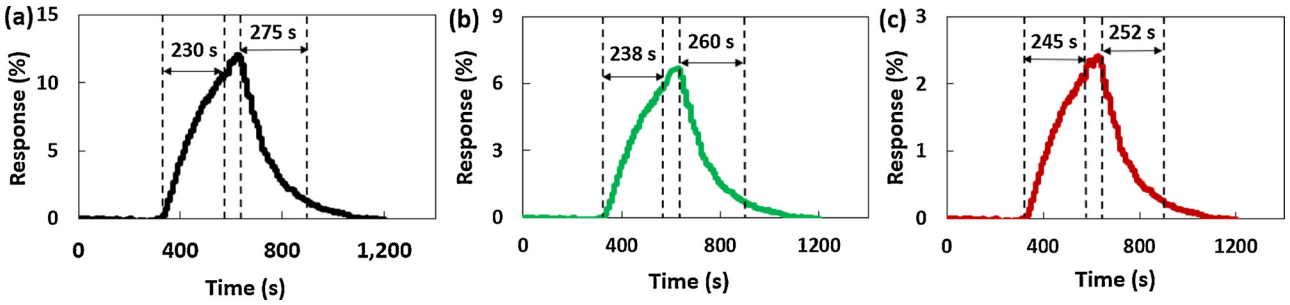

Fig. 7. Response and recovery curves of (a) ZnO/GaN device, (b) WO_3/GaN device, and.
(c) SnO_2/GaN device when exposed to 10 ppm of SO_2 in dry air under UV light at room temperature (20 °C).

energy and DOS calculations. However, recovery for the ZnO device was slightly slower than the other two metal oxide sensors. Recovery of gas molecules from the sensor surface becomes sluggish when the adsorption system is highly chemically stable because of possessing excessive adsorption energy. Furthermore, SnO_2 sensor device was found to be the fastest in SO_2 gas recovery-process due to exhibiting weaker chemical interaction, i.e., lower adsorption energy with SO_2 molecules. Therefore, neither strong nor weak chemical interaction between analyte and sensing surface is favorable to attain a quick responding sensor device.

The results from gas sensing data, response fitting lines and response-recovery transients indicate that ZnO-based sensor can be screened out as the optimal SO_2 sensor device among the three metal-oxide/GaN sensors considered. To further examine the ZnO sensor, its additional sensing properties, including gas sensing adsorption and desorption rate, cross-sensitivity to interfering gases, and long-term stability at various environmental conditions were investigated.

To study the adsorption and desorption of SO_2 molecules on ZnO, absorption/desorption rate constants (τ) were obtained from curve fitting of the first-order rate equation with experimental response data. The first-order rate equation is given by [29]:

$$R = R_f + (R_o - R_f)\, e^{-t/\tau} \quad (2)$$

where R is the instantaneous resistance, R_f is the final resistance after the end of an adsorption /desorption period, R_o is the initial resistance before an adsorption/desorption period, and t is the time. Fig. 8(a) presents measured resistance decrease associated with gas desorption and the fitted curve when the sensor had been allowed to recover after being exposed to 10 ppm SO_2. The experimental and fitted exponential curve are quite matched with a fitting error of ~4.8 %, which reveals the existence of a single rate constant, i.e., one charge transfer mechanism is mainly involved with the SO_2 response/recovery in ZnO sensor.

We know, adsorption/desorption rate constant (τ) indicates the speed of the gas adsorption /desorption process. The estimated adsorption and desorption rate constants at various SO_2 concentrations are showed in Fig. 8(b). It is found that, rate constants keep decreasing initially with the increase of SO_2 concentration and become nearly constant at higher gas concentrations. Also, desorption rate gets slower than the corresponding adsorption rate with the increasing SO_2 concentration.

It is well known that metal oxides are highly cross-sensitive to interfering gases present in the background of the target gas. In order to evaluate the selectivity, the ZnO sensor had been exposed to various background gases of SO_2 at three different levels of concentration at room temperature (20 °C). Fig. 8(c) demonstrates that the sensor is highly selective against hydrogen (H_2), methane (CH_4) and carbon dioxide (CO_2) at all levels of test concentration. The sensor showed some response toward nitrogen dioxide (NO_2) which can contribute minor cross-sensitivity to SO_2 response if present in the background. The cross-sensitive feature of ZnO mainly arises from the similar charge transfer process with SO_2 and NO_2, which was further addressed by applying principal component analysis (PCA) technique on the experimental gas response data.

Major transient response quantities, such as response magnitude, response time and recovery time are used as input parameters in PCA analyses. For the two test gases (SO_2 and NO_2), we collected gas responses for 6 different concentrations (0.5, 1, 10, 50, 100 and 500 ppm), and repeated the measurements 3 times. The input PCA dataset was a 36 × 3 matrix in which 60 % had been used as training set and 40 % was applied as test set. The component analyses comprised a variance threshold of 98 %. Fig. 8(d) shows the PC2 vs PC1 plot which includes up to 96 % of the total variance. All the raw data processing and PCA-analysis had been performed in the RapidMiner studio software.

The long-term stability is considered as the most vital parameter of sensors on which reliability of sensor device is dependent. The fabricated ZnO sensor devices showed excellent stability at room temperature and humidity. To further verify the stability and reliability, the fabricated devices had been stressed at harsh environmental conditions. For a consecutive 20 days, ZnO sensor devices were kept in four extreme environmental conditions such as: (1) low temperature (5 °C) and low humidity (5% RH), (2) low temperature (5 °C) and high humidity (90 % RH), (3) high temperature (100 °C) and low humidity (5% RH), and (4) high temperature (100 °C) and high humidity (90 % RH). The gas response data were collected after every 4 days with 10 ppm of SO_2 exposure. It was found that normalized responses of the devices were quite stable on applying environmental conditions (1) and (4) as plotted in Fig. 9(a). Sensor responses had been degraded initially with condition (2) and then started to get stable in the long run. The device showed the same trend with condition (3) but in opposite direction, i.e., normalized responses were increasing. From the results of all these applied stress-conditions, it appears that the ZnO device can withstand the extreme operating environments with a minor stability degradation. Also, high temperature environment is favorable for enhancing sensor response, but highly humid condition degrades response. Fig. 9(b) shows the variation of steady state resistance and corresponding sensor response change to 10 ppm SO_2 under different relative humidity conditions ranging from 5 % to 80 % RH at 20 °C. It is clearly seen that sensor response toward SO_2 gas is slightly susceptible (< 2%) to operating humid conditions even though steady state resistance of the device decreases gradually up to 4%.

Table 1 summarizes the comparison of SO_2 sensing performance of ZnO/GaN sensor with other recently reported SO_2 sensors. We utilized top-down fabrication approach comprising of optimized and well controlled process steps for the development of our devices. This enhances the scope of large-scale production of this device at low cost. Furthermore, the ZnO sensor possesses the advantages of low power consumption, low working temperature, strong response, excellent selectivity, stability at harsh conditions, and reproducibility which make this device suitable for the integration in multipurpose embedded chips.

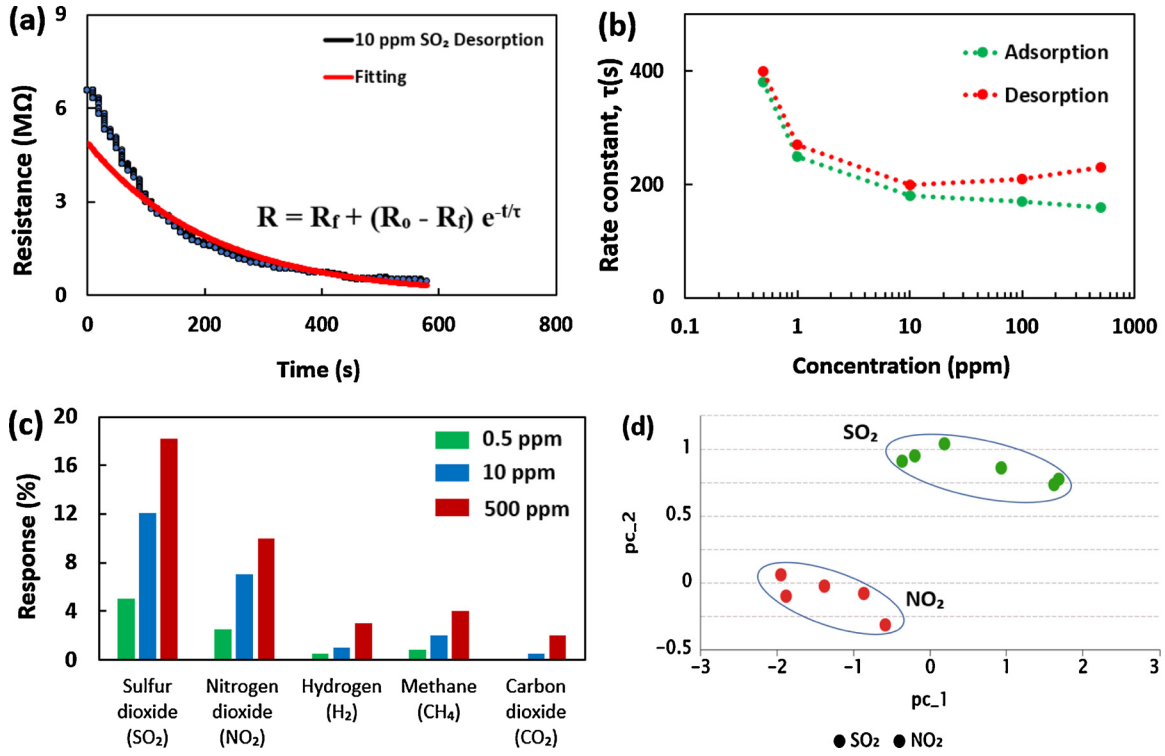

Fig. 8. (a) Decrease of resistance associated with gas desorption and the fitted curve when ZnO/GaN sensor had been allowed to recover after being exposed to 10 ppm SO_2 under dry air at 20°C. (b) Rate constant (τ) extracted from curve fitting vs SO_2 concentration in ppm. (c) Gas selectivity test for ZnO/GaN sensor toward various background gases at test concentrations of 0.5, 10 and 500 ppm of each gas at 20°C. (d) Principal Component Analysis: PC_2 vs PC_1 plot for 6 different concentrations of SO_2 and NO_2 gases exposed to ZnO sensor, which includes up to 96 % of the total variance.

4. Gas sensing mechanism

Under UV excitation with an energy above the bandgap energy, electron–hole pairs are generated both in the GaN and in the metal-oxide. Since photogenerated holes diffuse toward the GaN surface due to the surface band bending, carrier lifetime and thus the photocurrent increases within GaN nanowire. On the other hand, the chemisorbed oxygen and water molecules on metal-oxide receptors receive the photogenerated holes and get desorbed. SO_2 molecules are directly adsorbed onto these freshly produced sites due to their electrophilic property. This charge transfer between the metal-oxide and the SO_2 molecules raises the depletion region width within the GaN, thus decreases the sensor current. In this way, the device response is modulated with the depletion region alteration caused by the change in SO_2 gas concentration.

Since SO_2 is an oxidizing gas, it makes competitive adsorption on metal-oxides against aerial oxygen. The adsorbed aerial O_2 molecules are reduced to different oxygenated anionic species (O-, O_2-, O_2^{2-}, O^{2-}) by the extraction of free electrons from the metal-oxide surface. Some target SO_2 molecules combine with these oxygenated anionic species and oxidized to SO_3 molecules, contributing a sensor current modulation in opposite direction. Therefore, the overall sensor response is slightly degraded due to the competitive adsorption of aerial oxygen.

A schematic energy-band diagram of the metal-oxide/GaN and SO_2 molecule is illustrated in Fig. 10. Here, Fermi energy of the metal-oxide/GaN starts going down toward valence band as electrons are transferred from the metal oxide to the SO_2 molecule. This charge transfer process comes to an end when an equilibrium Fermi energy (E_{F_EQ}) is established in the adsorption system.

5. Conclusion

In this paper, we report the fabrication and characterization of metal oxide functionalized GaN nanowire on Si substrate using production standard stepper lithography for SO_2 gas detection. Three different functionalized devices, such as- ZnO/GaN, WO_3/GaN and SnO_2/GaN were prepared and their composition, crystallinity, surface topography and morphology were thoroughly examined. The gas sensing data was obtained and analyzed for all three sensors, and ZnO/GaN was appeared as the ideal sensor for high performance SO_2 sensing. The additional sensing properties of ZnO/GaN device such as- adsorption and desorption rate, cross-sensitivity to interfering gases, and long-term stability at extreme environmental conditions were investigated to confirm its implementation in field conditions. Using the energy band diagram, SO_2 gas sensing mechanism on the metal-oxide/GaN was explained in detail. Results indicate that ZnO/GaN sensor is a promising candidate for high performance SO_2 sensing in real-world applications.

Credit author statement

Md Ashfaque Hossain Khan: Conceptualization, Methodology, Fabrication, Software, Formal Analysis, Writing- Original draft preparation, Investigation, Writing - Review & Editing.
Brian Thomson: Resources, Validation.
Jie Yu: Material Characterization.
Ratan Debnath: Device Fabrication.
Abhishek Motayed: Conceptualization.
Mulpuri V. Rao: Supervision, Writing - Review & Editing.

Declaration of Competing Interest

There are no conflicts of interest to declare.

Acknowledgments

This work was sponsored through the National Science Foundation

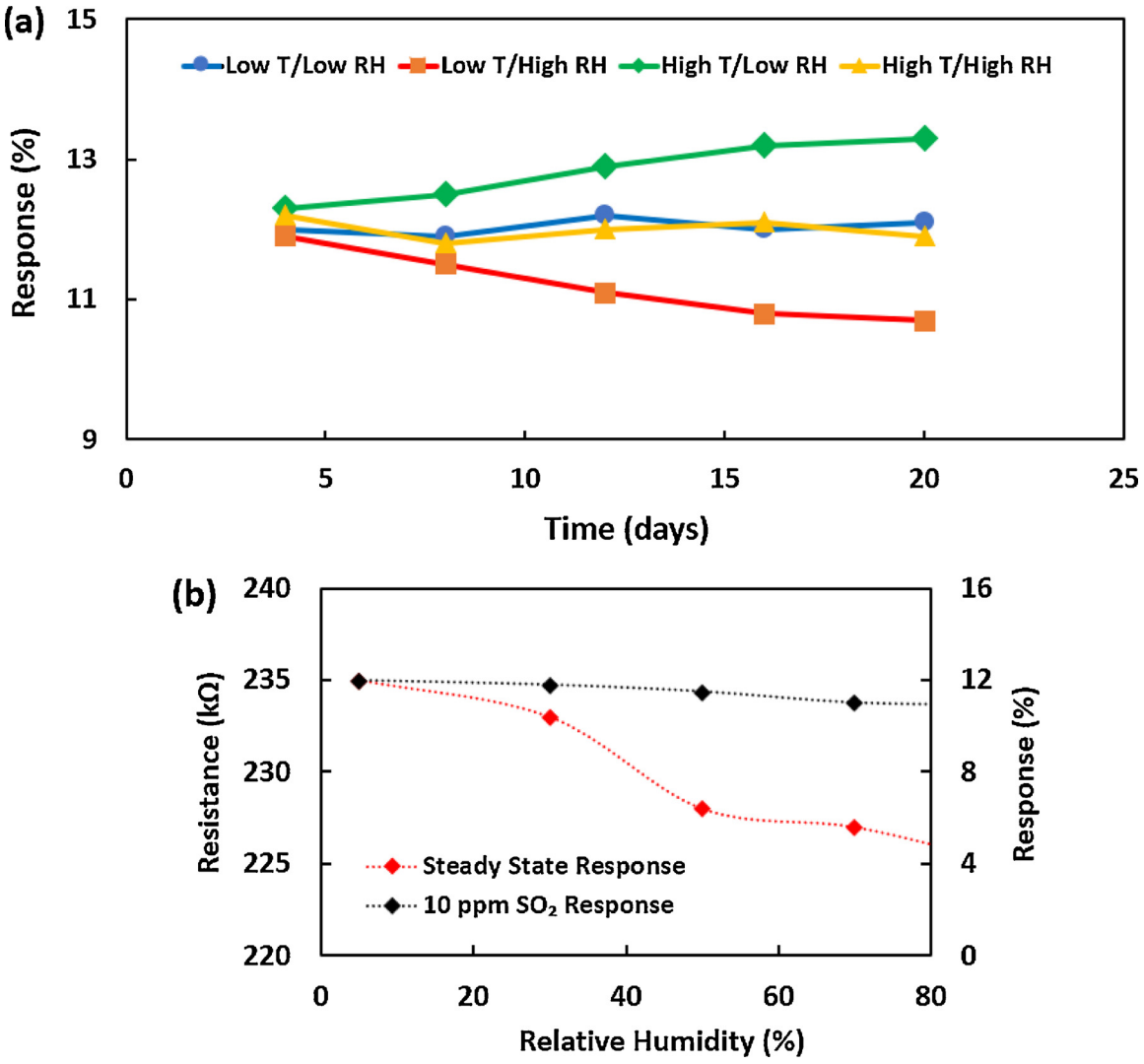

Fig. 9. (a) Long-term stability test of the ZnO/GaN devices at four different extreme environmental conditions stressed for 20 consecutive days. Low T = 5°C, High T = 100°C, Low RH = 5% RH, and High RH = 90 % RH. T and RH indicate temperature and relative humidity, respectively. (b) Steady state resistance change (red) and sensor response of ZnO device to 10 ppm SO_2 (black) for varying relative humidity conditions at 20°C. (For interpretation of the references to colour in this figure legend, the reader is referred to the web version of this article.)

Table 1
Comparison of gas sensing performance of ZnO/GaN sensor with other recently reported SO_2 sensors.

Materials	Structure	Operating Temperature (°C)	Concentration (ppm)	Sensitivity/ Response	Response time (s)	Recovery time (s)
ZnO/GaN [This work]	Nanowire	RT	10	12.1	230	275
Ni-MoS_2 [12]	Nanoflower	RT	5	7.4	50	56
NiO-ZnO [14]	Nanodisks	240	20	16.25	52	41
NiO/SnO_2 [15]	Thin film	180	500	56	80	70
Au/ZnO [30]	Thin films	RT	10	1.1	20 min	50 min
SnO_2-TiO_2 [31]	Composite (75 mol% of TiO_2)	450	10	55	5 min	> 5min
g- C_3N_4/rGO [32]	2D stacking hybrid	RT	2	0.0032 ppm^{-1}	140	130
SnO_2 [33]	Thin films	RT	1	138	–	–
TiO_2/rGO [34]	Nanocomposite	RT	1	10.08	73	128
Ru/Al_2O_3/ZnO [35]	Nanosheets	350	25	20	60	6 min
$SrMoO_4$ [36]	Nanoflowers	600	2000	−17.2	15.6 min	< 30 min
0.5 wt% Nb-WO_3 [37]	Nanorod	250	500	10	6	Several mins
RGO-ZnO on 2DEG AlGaN/GaN [38]	Nanorods	RT	120 ppb	14	120	320
CoZn-NCNTs [39]	Nanotube	RT	0.5	8.45%	32	900
Au-PANI [40]	Heterostructured thin film	RT	2	300	–	–
Polyaniline [41]	Nanoneedles	RT	10	4.2	180	< 180
Polyaniline-WO_3 [42]	Nanocomposite	RT	10	10.6	180	180
Polyaniline [43]	Porous nanofibers	RT	5	4.5%	185	< 200

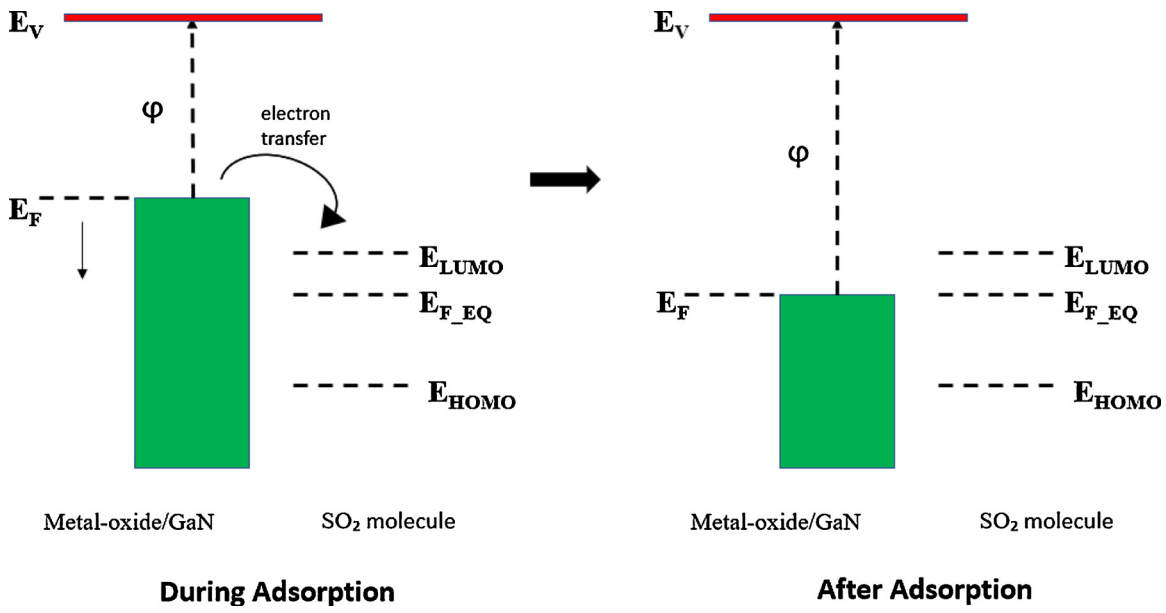

Fig. 10. Schematic representation of charge transfer mechanism within the energy band diagram of metal-oxide/GaN and SO_2 molecule. Here, ϕ, E_V, E_F and E_{F_EQ} represent work function of the metal oxide/GaN, energy of vacuum level, Fermi energy of the metal-oxide/GaN, and the equilibrium state of the adsorption system, respectively. E_{LUMO} and E_{HOMO} indicate the orbital energies of SO_2 molecule.

(NSF), USA Grant: ECCS1840712. The metal-oxide/GaN NW based SO_2 gas sensing devices were fabricated in the Nanofab of the NIST Center for Nanoscale Science and Technology. Gas sensing measurements were conducted at N5 Sensors, Inc.

Appendix A. Supplementary data

Supplementary material related to this article can be found, in the online version, at doi:https://doi.org/10.1016/j.snb.2020.128223.

References

[1] https://www.epa.gov/criteria-air-pollutants/naaqs-table#4.
[2] C. Chatterjee, A. Sen, Sensitive colorimetric sensors for visual detection of carbon dioxide and sulfur dioxide, J. Mater. Chem. A 3 (10) (2015) 5642–5647, https://doi.org/10.1039/C4TA06321J.
[3] R.R. Khan, M.J.A. Siddiqui, Review on effects of particulates; sulfur dioxide and nitrogen dioxide on human health, Int. Res. J. Environ. Sci. 3 (2014) 70–73.
[4] P. Roy, A. Sardar, SO2 emission control and finding a way out to produce sulphuric acid from industrial SO2 emission, J. Chem. Eng. Process Technol. 6 (2) (2015) 230.
[5] I. Levitsky, Porous silicon structures as optical gas sensors, Sensors 15 (8) (2015) 19968–19991, https://doi.org/10.3390/s150819968.
[6] B. Hök, B. Blückert, J. Löfving, Acoustic gas sensor with ppm resolution, Sens. Rev. 20 (2) (2000) 139–142.
[7] M. Li, et al., Nanoelectromechanical resonator arrays for ultrafast, gas-phase chromatographic chemical analysis, Nano Lett. 10 (10) (2010) 3899–3903, https://doi.org/10.1021/nl101586s.
[8] Z. Yunusa, Mohd.N. Hamidon, A. Kaiser, Z. Awang, Gas sensors: a review, Sens. Transd. 168 (4) (2014) 61–75.
[9] A. Rani, K. DiCamillo, M.A.H. Khan, M. Paranjape, M.E. Zaghloul, Tuning the polarity of $MoTe_2$ FETs by varying the channel thickness for gas-sensing applications, Sensors 19 (11) (2019) 2551, https://doi.org/10.3390/s19112551.
[10] M. Khan, M. Rao, Q. Li, Recent Advances in Electrochemical Sensors for Detecting Toxic Gases: NO_2, SO_2 and H_2S, Sensors 19 (4) (2019) 905, https://doi.org/10.3390/s19040905.
[11] D. Zhang, J. Liu, C. Jiang, P. Li, Y. Sun, High-performance sulfur dioxide sensing properties of layer-by-layer self-assembled titania-modified graphene hybrid nanocomposite, Sens. Actuators B Chem. 245 (2017) 560–567, https://doi.org/10.1016/j.snb.2017.01.200.
[12] D. Zhang, J. Wu, P. Li, Y. Cao, Room-temperature SO_2 gas-sensing properties based on a metal-doped MoS_2 nanoflower: an experimental and density functional theory investigation, J. Mater. Chem. A 5 (39) (2017) 20666–20677, https://doi.org/10.1039/C7TA07001B.
[13] P. Tyagi, A. Sharma, M. Tomar, V. Gupta, Low temperature operated NiO-SnO2 heterostructured SO2 gas sensor, Presented at the 5TH National Conference on Thermophysical Properties: (NCTP-09), Baroda (India), 2016, p. 020077, , https://doi.org/10.1063/1.4945197.
[14] Q. Zhou, W. Zeng, W. Chen, L. Xu, R. Kumar, A. Umar, High sensitive and low-concentration sulfur dioxide (SO2) gas sensor application of heterostructure NiO-ZnO nanodisks, Sens. Actuators B Chem. 298 (2019) 126870, https://doi.org/10.1016/j.snb.2019.126870.
[15] E. Çiftyürek, K. Sabolsky, E.M. Sabolsky, Molybdenum and tungsten oxide based gas sensors for high temperature detection of environmentally hazardous sulfur species, Sens. Actuators B Chem. 237 (2016) 262–274, https://doi.org/10.1016/j.snb.2016.06.071.
[16] J.Y. Tsao, et al., Ultrawide-bandgap semiconductors: research opportunities and challenges, Adv. Electron. Mater. 4 (1) (2018) 1600501, https://doi.org/10.1002/aelm.201600501.
[17] C. Jagadish, S.J. Pearton (Eds.), Zinc Oxide Bulk, Thin Films and Nanostructures: Processing, Properties and Applications, Elsevier, Amsterdam; Boston, 2006.
[18] G.S. Aluri, et al., Highly selective GaN-nanowire/TiO_2 -nanocluster hybrid sensors for detection of benzene and related environment pollutants, Nanotechnology 22 (29) (2011) 295503, https://doi.org/10.1088/0957-4484/22/29/295503.
[19] M.A.H. Khan, B. Thomson, R. Debnath, A. Motayed, M.V. Rao, Nanowire-based sensor array for detection of cross-sensitive gases using PCA and machine learning algorithms, IEEE Sens. J. (2020) 1, https://doi.org/10.1109/JSEN.2020.2972542.
[20] G.S. Aluri, A. Motayed, A.V. Davydov, V.P. Oleshko, K.A. Bertness, M.V. Rao, Nitro-aromatic explosive sensing using GaN nanowire-titania nanocluster hybrids, IEEE Sens. J. 13 (5) (2013) 1883–1888, https://doi.org/10.1109/JSEN.2013.2241423.
[21] M.A.H. Khan, B. Thomson, A. Motayed, Q. Li, M.V. Rao, Functionalization of GaN nanowire sensors with metal oxides: an experimental and DFT investigation, IEEE Sens. J. (2020) 1, https://doi.org/10.1109/JSEN.2020.2978221.
[22] E. Muchuweni, T.S. Sathiaraj, H. Nyakotyo, Synthesis and characterization of zinc oxide thin films for optoelectronic applications, Heliyon 3 (4) (2017) e00285, https://doi.org/10.1016/j.heliyon.2017.e00285.
[23] M. Aslan, Preparation of c-axis-oriented zinc-oxide thin films and the study of their microstructure and optical properties, Sol. Energy Mater. Sol. Cells (2004), https://doi.org/10.1016/j.solmat.2003.06.016.
[24] B. Cullity, Elements of X-ray Diffraction, Prentice hall, New Jersey, 2001.
[25] T. Xie, et al., The effects of surface conditions of TiO_2 thin film on the UV assisted sensing response at room temperature, Thin Solid Films 620 (2016) 76–81, https://doi.org/10.1016/j.tsf.2016.07.075.
[26] T.K. Zywietz, J. Neugebauer, M. Scheffler, The adsorption of oxygen at GaN surfaces, Appl. Phys. Lett. 74 (12) (1999) 1695–1697, https://doi.org/10.1063/1.123658.
[27] M.A.H. Khan, B. Thomson, R. Debnath, A. Rani, A. Motayed, M.V. Rao, Reliable Anatase-Titania Nanoclusters Functionalized GaN Sensor Devices for UV assisted NO_2 Gas-Sensing in ppb level, Nanotechnology (2019), https://doi.org/10.1088/1361-6528/ab6685.
[28] N. Yamazoe, K. Shimanoe, Theory of power laws for semiconductor gas sensors, Sens. Actuators B Chem. 128 (2) (2008) 566–573, https://doi.org/10.1016/j.snb.2007.07.036.
[29] Y. Zhang, A. Kolmakov, S. Chretien, H. Metiu, M. Moskovits, Control of catalytic reactions at the surface of a metal oxide nanowire by manipulating Electron density inside it, Nano Lett. 4 (3) (2004) 403–407, https://doi.org/10.1021/nl034968f.
[30] A. Gaiardo, et al., ZnO and Au/ZnO thin films: room-temperature chemoresistive properties for gas sensing applications, Sens. Actuators B Chem. 237 (2016) 1085–1094, https://doi.org/10.1016/j.snb.2016.07.134.
[31] S. Mulmi, V. Thangadurai, Semiconducting SnO_2-TiO_2 (S-T) composites for detection of SO_2 gas, Ionics 22 (10) (2016) 1927–1935, https://doi.org/10.1007/

s11581-016-1711-4.
[32] A. Chen, R. Liu, X. Peng, Q. Chen, J. Wu, 2D hybrid nanomaterials for selective detection of NO_2 and SO_2 using 'Light on and off' strategy, ACS Appl. Mater. Interfaces 9 (42) (2017) 37191–37200, https://doi.org/10.1021/acsami.7b11244.
[33] C.A. Betty, S. Choudhury, Charge carrier transport in nanocrystalline SnO2 thin film sensor and temperature dependence of toxic gas sensitivity, Sens. Actuators B Chem. 237 (2016) 787–794, https://doi.org/10.1016/j.snb.2016.06.163.
[34] V. Petryshak, Highly sensitive active medium of primary converter SO2 sensors based on cholesteric-nematic mixtures, doped by carbon nanotubes, Electrotech. Rev. 1 (3) (2017) 119–122, https://doi.org/10.15199/48.2017.03.27.
[35] D.L. West, F.C. Montgomery, B.L. Armstrong, Compact, DC-electrical biased sulfur dioxide sensing elements for use at high temperatures, Sens. Actuators B Chem. 162 (1) (2012) 409–417, https://doi.org/10.1016/j.snb.2012.01.001.
[36] Y. Liu, et al., An integrated micro-chip with Ru/Al2O3/ZnO as sensing material for SO2 detection, Sens. Actuators B Chem. 262 (2018) 26–34, https://doi.org/10.1016/j.snb.2018.01.156.
[37] V. Kruefu, A. Wisitsoraat, S. Phanichphant, Effects of niobium-loading on sulfur dioxide gas-sensing characteristics of hydrothermally prepared tungsten oxide thick film, J. Nanomater. 2015 (2015) 1–8, https://doi.org/10.1155/2015/820509.
[38] J.P. Stephen, Gallium Nitride Processing for Electronics, Sensors and Spintronics, Springer, London, UK, 2006.
[39] P. Choeichom, A. Sirivat, Discriminative sensing performances of ZSM-5, Y, mordenite, ferrierite, beta, 3A, 4A, 5A, and 13X zeolites towards sulfur dioxide, Ionics 24 (9) (2018) 2829–2841, https://doi.org/10.1007/s11581-017-2422-1.
[40] C.A. Betty, S. Choudhury, S. Arora, Tin oxide–polyaniline heterostructure sensors for highly sensitive and selective detection of toxic gases at room temperature, Sens. Actuators B Chem. 220 (2015) 288–294, https://doi.org/10.1016/j.snb.2015.05.074.
[41] V. Chaudhary, A. Kaur, Solitary surfactant assisted morphology dependent chemiresistive polyaniline sensors for room temperature monitoring of low parts per million sulfur dioxide: Polyaniline sensors for monitoring SO_2, Polym. Int. 64 (10) (2015) 1475–1481, https://doi.org/10.1002/pi.4944.
[42] V. Chaudhary, A. Kaur, Enhanced room temperature sulfur dioxide sensing behaviour of in situ polymerized polyaniline–tungsten oxide nanocomposite possessing honeycomb morphology, RSC Adv. 5 (90) (2015) 73535–73544, https://doi.org/10.1039/C5RA08275G.
[43] V. Chaudhary, H. Singh, A. Kaur, Effect of charge carrier transport on sulfur dioxide monitoring performance of highly porous polyaniline nanofibres: Charge carrier transport effect on SO_2 monitoring performance of PAN nanofibres, Polym. Int. 66 (5) (2017) 699–704, https://doi.org/10.1002/pi.5311.

Md Ashfaque Hossain Khan received his B.Sc. degree in Electrical and Electronic Engineering in 2015 from Bangladesh University of Engineering and Technology, Dhaka, Bangladesh. He is currently pursuing a Ph.D. degree in Electrical Engineering at The George Mason University, Fairfax, VA, USA. He has been working as a guest researcher in the Nanofab of the NIST Center for Nanoscale Science and Technology since 2018. His current research interests include fabrication and measurement of semiconducting nanowire based electrical devices for chemical sensing.

Brian Thompson is a Senior Product Engineer at N5 Sensors. He is responsible for managing gas sensor testing, integration and product development. He has a master's degree in Technical Entrepreneurship and Management and a bachelor's degree in Chemical Engineering, both from University of Rochester.

Jie Yu received her Ph.D. degree in 2018 from the Chemical Engineering department at the University of Akron. During her graduate studies, she worked on in Situ IR study on the structure of adsorbed species on immobilized amines in CO_2 capture. She is currently working as a surface/catalyst scientist in N5 Sensors, Inc.

Ratan Debnath has extensive experience of functionalization of nanostructures using thiols which is the essential part of the proposed research and published over 10 articles in peer reviewed journals based on such work. He has received Dr.-Ing. (Doctor of Engineering) in Electrical Engineering from RWTH Aachen University of Technology and Research Center Jülich, Germany and completed his Bachelor of Engineering in Electronics & Communication, from Indian Institute of Technology, Roorkee, India. Debnath's professional experience involve Postdoctoral Fellowship at the University of Toronto, Canada, where he developed Schottky and hetero-junction junction solar cells using band gap tunable quantum dots. He also worked as NIST-ARRA Senior Fellow/Visiting Assistant Research Scientist, at National Institute of Standards and Technology, Gaithersburg and University of Maryland, College Park, USA, where he designed and constructed all back-contact 3D CdS/CdTe and CdSe/CdTe photovoltaic devices. Dr. Debnath (full-time employed by N5 Sensors, Inc.) has over 7 years of experience in various aspects nitride nanoscale structures, spanning from materials to devices. He has more than 40 publication with over 3600 citations.

Abhishek Motayed received his Ph.D. degree in 2007 from the Electrical and Computer Engineering department at the University of Maryland, College Park. During his graduate studies, he worked at the National Institute of Standards and Technology (NIST) as a guest scientist. Dr. Motayed continued working at NIST after graduating, with an appointment as a research scientist at the Institute of Research in Electronics and Applied Physics at the University of Maryland. His current research expertise and interests are high-performance nanoscale electronic/optical devices with emphasis on large-scale integration, novel chemical/biological/radiation sensor systems, energy conversion/storage, and bio-medical applications of nanoscale devices. Currently, he is the CEO of N5 sensors, Inc., Rockville, MD 20850, USA.

Mulpuri V. Rao received the B.Tech. degree in electronics and communication engineering from the College of Engineering, Kakinada, India, in 1977, the M.Tech. degree in material science from the Indian Institute of Technology Bombay, Mumbai, India, in 1979, and the M.S. and Ph.D. degrees in electrical engineering from Oregon State University, Corvallis, in 1983 and 1985, respectively. From 1979 to 1981, he was a Lecturer in electronics and communication engineering at Sidhartha Engineering College, Vijayawada, India. Since August 1984, he has been with George Mason University, Fairfax, VA, where he is currently a Professor in the Electrical and Computer Engineering Department. He is the author or coauthor of more than 120 articles published in various journals in the areas of epitaxial growth, ion implantation, ohmic contacts, material characterization, photodetectors, microwave and high-power devices, microfluidic cells, gas sensing, etc.